Journal of Magnetism and Magnetic Materials 607 (2024) 172407

Contents lists available at ScienceDirect

Journal of Magnetism and Magnetic Materials

journal homepage: www.elsevier.com/locate/jmmm

Research article

Magnetocaloric effect properties in the Ashkin–Teller model

J.P. Santos [a,b,e,*], R.H.M. Morais [a,c], R.M. Francisco [a,d], D.S. Rosa [d], E. Nepomuceno [e]

[a] Department of Natural Sciences, Federal University of São João del-Rei (UFSJ), MG, Brazil
[b] Department of Mathematics, Federal University of São João del-Rei (UFSJ), MG, Brazil
[c] Department of Science and Languages, Federal Institute of Education, Science and Technology of Minas Gerais (IFMG), Brazil
[d] Department of Physics, Aeronautics Technological Institute (ITA), SP, Brazil
[e] Department of Electronic Engineering, Maynooth University, Maynooth, Ireland

ARTICLE INFO

Keywords:
Magnetocaloric effect
Mean-field theory
Ashkin–Teller model
Phase transition
Isothermal entropy change

ABSTRACT

This work investigates magnetic properties and the magnetocaloric effect in the scope of continuous and first-order phase transitions in different stability regimes of a system described by the Ashkin–Teller model. Mean Field Theory is implemented through the Gibbs–Bogoliubov variational principle to obtain expressions for free energy, entropy and magnetization, in addition to computing the magnetocaloric properties of the system under analysis. The starting point is a detailed analysis of magnetic properties as a function of temperature, coupling configurations and external fields. Continuous and first-order phase transitions are observed. The impact of having the system under the influence of an external field is studied, showing and discussing the most favorable conditions for the manifestation of the magnetocaloric potential. In addition, phase transitions between metastable and stable states due to the hysteresis effect when varying the external field are obtained from two different methods, Maxwell relations and the use of entropy variation to compute the correct magnetocaloric effect properties.

1. Introduction

Observed by E. Warburg [1] in 1881, the magnetocaloric effect (MCE) is a physical phenomenon in which the temperature of some materials changes when the system is driven from a initial to a final state under the influence of a variation in the external magnetic field applied to it. This behavior was also observed years latter by Weiss and Picard [2] and can be calculated by means of an adiabatic variation of temperature or an isotermic variation of the magnetic entropy of the material under study [3]. MCE has become a major research topic due to its diversity of results regarding the magnetic properties of materials. We realized this when analyzing theoretical works on the subject such as that of Guerrero [4] in which magentocaloric properties of the $J_x - J_y$ Blume–Capel model were obtained through the two point approximation of the Cluster Variation Method, finding different characteristics for the phase diagram according to the values of the anisotropic parameter, external magnetic field, temperature and ratio between exchange parameters, highlighting the discovery of direct and inverse MCE through the application of low fields and temperatures around jumps between plateaus of magnetization. Another example of recent theoretical work that we can cite is that of Mandal and collaborators [5], in which the researchers presented results on magnetocaloric properties on two series of double perovskites compounds $La_2FeMn_{1-x}Cu_xO_6$ and $Sr_2RuMn_{1-x}Fe_xO_6$ with different concentrations, showing that for certain doping levels of specific ions, there was a coexistence of direct and inverse MCE. Other examples of recent work in this line of theoretical analyzes can be seen in [6–9]. Furthermore, we can also mention recent works in lines of experimental research on the magnetocaloric effect, such as those by Ghorai et al. [10] in which the magentocaloric properties of the material $La_{0.4}Pr_{0.3}Ca_{0.1}Sr_{0.2}MnO_3$ were analyzed for possible applications in magnetic refrigeration at room temperature, and by Sharma and collaborators [11] in which, through XRD, structural, magnetic, and magnetocaloric properties of the perovskite $TmFeO_3$ were discovered, which showed hysteresis cycles with interesting characteristics of this material for application in magnetic refrigeration. Another interesting experimental work is that of Bouhbou et al. [12] in which magnetic, magnetocaloric and critical exponent properties of amorphous $Fe_{67}Y_{33}$ ribbons were investigated after preparing the material using melt-spinning method, making comparisons between the results obtained experimentally and theoretically, finding second-order phase transitions and critical exponents close to those of the long-range mean-field approach, confirming

* Corresponding author at: Department of Natural Sciences, Federal University of São João del-Rei (UFSJ), MG, Brazil.
E-mail addresses: jander@ufsj.edu.br (J.P. Santos), rubens_henrique3945@aluno.ufsj.edu.br (R.H.M. Morais), rafaelrmf@ita.br (R.M. Francisco), derickdsr@ita.br (D.S. Rosa), erivelton.nepomuceno@mu.ie (E. Nepomuceno).

https://doi.org/10.1016/j.jmmm.2024.172407
Received 21 March 2024; Received in revised form 30 June 2024; Accepted 5 August 2024
Available online 10 August 2024

the validity of this type of approximation. In addition to these works, other experimental studies on magnetocaloric potentials can be seen in [13–16].

As a phenomenon that falls within the research field of areas such as thermodynamics, statistical and quantum mechanics, an effective way to study the MCE is through spin models, since they are capable of modeling the structure of certain magnetic materials and thus allow the investigation of their properties and its relation with temperature and external fields. To this end, several approximation theories can be applied to such models, of which we can mention the Mean Field Theory (MFT), a widely disseminated method in the study of materials, as in the work of Oliveira and collaborators [17] in which they investigated MCE properties of the spin-1 Blume–Capel model in a hexagonal lattice through MFT, analyzing the characteristics of the free energy, magnetization and entropy of the system for critical exponents in continuous and first-order phase transitions. Another recent work that we can mention here that also makes use of this approach is that of Abu-Elmagd et al. [18] in which through MFT and first-principles DFT calculation the authors investigated the magnetocaloric effect in YFe_3 and $HoFe_3$ compounds, analyzing that the nature of the phase transition of these materials belongs to the class of second order, in agreement with the universal MCE curve of YFe_3. Still on current applications of this method, we can mention the work of Mounira, Zaidi and Hlil [19] in which MFT was used to establish the magnetocaloric properties in TbFeSi and DyFeSi intermetallic magnetic alloys, finding convergences between theoretical results and experimental literature. Therefore, as mentioned previously, Mean Field Theory is widely used in the area of materials research, being present in several recent works, as can still be seen in the following Refs. [20–26]. Another approximation method applicable to spin models for studying thermodynamic and magnetic properties of materials is the Effective Field Theory (EFT), which was recently used by Morais, Santos and Sá Barreto [27] in obtaining results of such properties of a graphene-type nanostructure with ABA stacking described by the q-state Potts model, investigating the magnetization, the free energy, the internal energy, the entropy, and the specific heat of this system, concluding the presence of second and first-order phase transitions depending on the number of states. Another research in which Effective Field Theory was used is by Ümit Akıncı [28], in which properties of the MCE of Ising binary alloys with arbitrary spin values and different concentrations were obtained through EFT, showing that different spin and concentration values can tune the magnetocaloric performance and increase the refrigerant capacity. Effective Field Theory, as well as Mean Field Theory, is widely used as an approximation method in the study of material properties, and other recent works with applications can be seen in [29–33]. A last example of these approximation methods that we can mention is the Monte Carlo Simulation (MC), used in works such as that of Kadim and collaborators [34] in which using the Ab initio and Monte Carlo calculations, the authors studied magnetocaloric properties of $La_{0.75}Sr_{0.25}MnO_3$ perovskite, showing that such material is a good candidate for applications in magnetic refrigeration at ambient temperatures and with the application of moderate external fields. Another example is that of Yang et al. [35] in which the thermodynamic properties and the magneotcaloric effect of a polyhedron chain with mixed spin were studied using MC simulation, concluding that parameters such as exchange coupling, spin quantum number and external magnetic field play an important role in the effects on the compensation behavior of the ferrimagnetic system. Other recent works that use MC simulation can be seen in [36–38].

Experimental and theoretical works in the literature has investigated MCE with a focus on physical contexts where continuous phase transitions are presented, such as in the work of Zhang et al. [39], in which the researchers reported the presence of a giant magnetocaloric effect properties in all-*d*-metal Ni(Co)MnTi based magnetic Heusler alloys and analyzed the materials with results of second-order phase transitions. In parallel with this type of analysis, some methods for studying it in first-order phase transitions regimes have been proposed with the aim of taking into account the MCE contribution due to discontinuities in the magnetization, as in the work of Morais et al. [40] in which the characteristics of the magnetocaloric effect were analyzed within the scope of first-order phase transitions in a cubic lattice described by the q-state Potts model using EFT, highlighting the use of Maxwell relations in the analysis of the equilibrium behavior of the thermodynamic quantities and the Clausius–Clapeyron equation for cases with discontinuity in the order parameter. Another work that performs this type of analysis is that of Nascimento and collaborators [41] in which the magnetocaloric effect and properties such as free energy, magnetization and entropy are explored in the spin-3/2 Blume–Capel model using MFT for continuous and first order phase transitions. Some other works that also propose to perform the MCE analysis for first-order phase transitions in different contexts and objectives can be seen in [42–46]. In this context, a spin model that exhibits a rich phase diagram where both continuous and first-order phase transitions are present, besides many tricritical points and mixed phases, is the Ashkin-Teller model (AT model) [47]. This model was proposed in 1943 for description of the cooperative phenomena of quaternary alloys and can be seen as a generalization of the Ising model to a four-component system. Due to its potential application in various areas, such as magnetism [48,49], chemical interactions in metallic alloys [50], elastic response of DNA molecule to external force and torque [51] and phase diagram of selenium adsorbed on the Ni(100) surface [52], the AT model has, over time, been the subject of many works by means of different methods, such as MFT [53–58], EFT [59], rigorous inequality correlation function [60], renormalization group theory (RG) [61,62], mean-field renormalization group (MFRG) [63,64] and MC simulation [65–67]. Recently, the stability properties of systems described by this model were studied based on the application of external fields oscillating over time [68] and under the analysis of the critical exponents of the free energy values of the system [69], thus enabling the investigation of conditions of the parameters applied to the model that allow the emergence of stable, metastable and unstable states.

As mentioned, this model has a variety of results related to lattice statistics problems and the analysis of the critical behavior of systems, and can be used in the modeling of materials, as in the case of the work of Benmansour and collaborators [70], in which ferromagnetic thin films were modeled from the AT model, obtaining magnetic properties and phase diagrams of this theoretical material in the presence of a crystal field. In addition, some materials may present exchange interaction systems, critical behaviors and phase transition phenomena similar to those found in the study of this model, as in the case of the work by Kumar et al. [71], in which the AT model was mentioned in an attempt to explain the existence of fourfold vertices in ferroelectrics in ultra-tetragonal $PbTiO_3$ thin films, or in the case of the work of Varma and Zhu [72], who mentions the fact that thermodynamic properties of the loop current order transitions with broken symmetry in high-temperature superconductors exhibit characteristics of AT model properties. Therefore, whether in the direct application in the description of the spin variables of a lattice capable of modeling the structure of a material or for the explanation of critical phenomena and phase transition that arise from the study of different types of systems, it is necessary to better understand the properties of the Ashkin-Teller model in order to use it more accurately, thus justifying new studies regarding the results of the lattice statistics of this model.

In light of the above, in this work we aim to study the MCE properties of the AT model in a cubic lattice by means of the MFT from the Gibbs-Bogoliubov variational principle [73–75]. To accomplish this, first, we obtain some thermodynamic quantities, such as free energy, entropy and magnetization. Then, we plot some phase diagrams and obtain the critical parameters of the system, so that we can know which method to use in each critical regime, i.e., continuous and first-order phase transition. With this information in hand, we calculate the variation of magnetic entropy of the system with respect to the

variation in the external field applied to it, using the Maxwell relation where only continuous variations for the magnetization are present and the Clausius–Clapeyron equation where first-order phase transitions take place. To finalize the study, we investigate the MCE related to the first-order phase transitions that occur for the metastable states of the system due to hysteresis effects and compare it to some results obtained by Amaral et al. [76].

We can highlight here that the MFT approach is used in this work as an initial tool suitable for a preliminary understanding of the problem. Although it is known that the MFT approach does not produce results as accurate as other numerical and analytical methods, it serves as a first qualitative insight into the problem.

The article is organized as follows. In Section 2, we present the mathematical formalism used to investigate the system. In Section 3, we analyze the numerical results and diagrams that were obtained. In Section 4, we conclude and make the conclusions.

2. Model and formulation

This section aims to present conceptual aspects and the mathematical formalism necessary to understand the means by which the results presented in Section 3 were obtained. This work studies the spin-1/2 Ashkin-Teller model, which establishes the construction of an Ising-type system composed of the spin variables S and σ that are coupled by an exchange interaction J and a third variable σS coupled by the exchange interaction K. Let us therefore begin with the presentation of the Hamiltonian of this system

$$H = -\sum_{\langle ij\rangle}\left[J\left(S_iS_j+\sigma_i\sigma_j\right)+KS_i\sigma_iS_j\sigma_j\right]-h\sum_i\left(S_i+\sigma_i+S_i\sigma_i\right), \tag{1}$$

where the term $\langle ij\rangle$ denotes the idea of interaction between pairs of nearest neighboring spins and h is an external magnetic field.

In this work we propose the development of MFT through a variational principle based on Bogoliubov's inequality [73–75], which consists of the validity of the following expression

$$G \le \phi = G_0 + \langle H - H_0\rangle_0 . \tag{2}$$

The total Hamiltonian of the lattice, denoted by H, describes the interactions among spin variables within the system, along with its corresponding free energy G. Meanwhile, H_0 represents the trial Hamiltonian of a simplified lattice-statistical model, enabling precise calculations, while G_0 stands for its associated free energy. Additionally, $\langle ...\rangle_0$ signifies the mean of the canonical ensemble within this simplification. Finally, ϕ characterizes the variational Gibbs free energy, offering an upper bound for the true Gibbs free energy due to this method.

The mathematical procedure of the MFT approximation used in this work requires us to construct a trial Hamiltonian with the presence of variational parameters. For our study, through the mathematical development of the MFT, the trial Hamiltonian for the spin-1/2 AT model is given by

$$H_0 = -\sum_k^N\left(S_k\gamma_S+\sigma_k\gamma_\sigma+\sigma_kS_k\gamma_{\sigma S}\right), \tag{3}$$

where γ_S, γ_σ and $\gamma_{\sigma S}$ are the variational parameters for each spin variable in the AT model, and N represents the number of sites present in the lattice. To simplify the mathematical formalism, for the rest of this work, we define the notation τ to represent the variables S, σ and σS, that is, $\tau = \{S, \sigma, \sigma S\}$.

The parameters γ_τ have a physical meaning, acting on localized spins on the i site with an effective field role that operates on its boundary. In order to obtain the thermodynamic quantities, we have to minimize the free energy of the model with respect to the these variational parameters, process that can also be seen in [17,41,53]. Then, we can write expressions for the Gibbs free energy (G) and magnetizations (m_τ) as

$$G = -Nk_BT\ln\left[4\left(\prod_{\{\tau\}}\cosh\beta\gamma_\tau+\prod_{\{\tau\}}\sinh\beta\gamma_\tau\right)\right]$$
$$+\frac{zN}{2}\left[Jm_S{}^2+Jm_\sigma{}^2+Km_{\sigma S}{}^2\right], \tag{4}$$

and

$$m_\tau = \frac{\tanh\beta\gamma_\tau+\tanh\beta\gamma_{\tau'}\tanh\beta\gamma_{\tau''}}{1+\tanh\beta\gamma_\tau\tanh\beta\gamma_{\tau'}\tanh\beta\gamma_{\tau''}}, \tag{5}$$

where the variational parameters are given by $\gamma_S = zJm_S + h$, $\gamma_\sigma = zJm_\sigma + h$ and $\gamma_{\sigma S} = zKm_{\sigma S} + h$. The notations τ' and τ'' were used to show that the variational parameters refer to different magnetizations ($\tau \neq \tau' \neq \tau''$) and z represents the coordination number of the lattice.

With these expressions in hand, we can establish the conditions for obtaining phase transition lines. For continuous transitions, we take the following condition $m_\tau \to 0$, while for the case of first order transitions we seek to establish the values for the equation $G(m_\tau) = G(m'_\tau)$, following the condition that $m_\tau \neq m'_\tau$.

From Eqs. (4) and (5), we obtain the entropy of the system

$$S = -\frac{\partial G}{\partial T}. \tag{6}$$

Now we can establish ways to calculate the entropy variation of the system $\Delta S_M(T, \Delta h)$, with M being the set of magnetizations ($M = \{m_S, m_\sigma, m_{\sigma S}\}$). The most direct and simple way is to subtract from the value of a final entropy state an initial state value through an isothermal process, i.e.,

$$\Delta S_M(T,\Delta h) = S_{M_2}(T,h_2) - S_{M_1}(T,h_1) \tag{7}$$

where M_1 and M_2 are different states that depend on the external field intensities h_1 and h_2.

Another way to obtain the magnetocaloric potential is to establish its value using the Maxwell relations of Eqs. (5) and (6) [77] solving the following integral

$$\Delta S_M(T,\Delta h) = \sum_{\{\tau\}}\int_{h_1}^{h_2}\left[\frac{\partial m_\tau(T,h)}{\partial T}\right]_h dh. \tag{8}$$

When first-order phase transitions take place, we have to add an extra term in Eq. (8) to compute its contribution in the entropy variation due to the magnetization discontinuity, as can be seen in the Refs. [17,40,41], so that this expression becomes

$$\Delta S_M^{(fo)}(T,\Delta h) \cong \sum_{\{\tau\}}\left\{\int_{h_1}^{h_C-\delta h}\left[\frac{\partial m_\tau(T,h)}{\partial T}\right]_h dh + \int_{h_C+\delta h}^{h_2}\left[\frac{\partial m_\tau(T,h)}{\partial T}\right]_h dh + \delta S_\tau\right\}, \tag{9}$$

where $\delta h \to 0$ and the notation (fo) indicates the presence of first-order phase transitions. To indicate the presence of this first-order phase transition, the subscript (C) will be used, for example, T_C and h_C. As we can observe, the expression given in Eq. (9) has three different terms, which provide the MCE exhibited by the system in a particular process before (first-term), after (second-term) and during (third-term) the occurrence of the first-order phase transition. The third-term will be obtained by means of the Clausius–Clapeyron equation, described as

$$\delta S_\tau = \left(\frac{dh}{dT}\right)\delta m_\tau(T_C,h_C), \tag{10}$$

where the variation in the order parameter (δm_τ) around T_C can be obtained by $\delta m_\tau(T_C,h_C) = m_{\tau_{(h_C-\delta h)}} - m_{\tau_{(h_C+\delta h)}}$.

3. Numerical results and diagrams

In this section, we show the magnetizations and MCE curves, besides phase diagrams for the AT model in a cubic lattice ($z = 6$). The first-order phase transitions exhibited by the system can be found between stable states, where $G(m_\tau) = G(m'_\tau)$, and also between metastable and unstable states, due to the hysteresis effect, both will be shown in the phase diagrams. For simplification here we will consider units of $k_B = 1$, $K/J = x$.

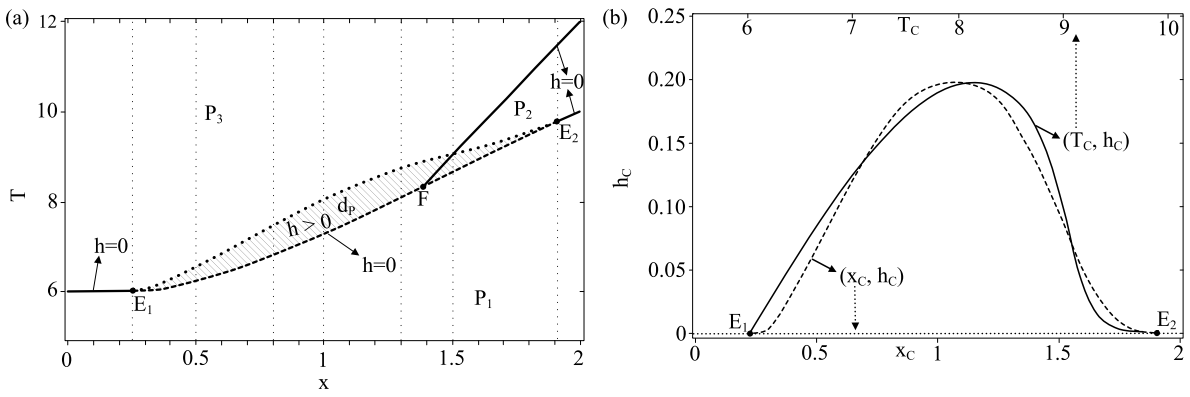

Fig. 1. (a) Phase diagram (T as function of $x = K/J$) of spin-1/2 AT model in a cubic lattice obtained from MFT approximation for null external field. Second order phase transitions are represented by solid lines, and the hatched region represents the values for which first-order phase transitions occur. (b) External field (h_C) as a function of the parameters (T_C) and (x_C), establishing the condition for the presence of first-order phase transitions, that is, the (d_P) phase.

In order to start the presentation of the numerical results, let us first define the notations used in this work for the phases obtained with different external field values ($h \geq 0$):

(i) The *Baxter*$^{(1)}$ phase is denoted by P_1, where $m_\tau^{(1)} \neq 0$, with $h = 0$. Considering $h > 0$, for $m_\tau^{(2)} > m_\tau^{(1)}$, this phase is denoted by *Baxter*$^{(2)}$.

(ii) The $\langle \sigma S \rangle^{(1)}$ phase is denoted by P_2, where $m_\sigma^{(1)} = m_S^{(1)} = 0$ and $m_{\sigma S}^{(1)} \neq 0$, with $h = 0$. Considering $h > 0$, for $m_\sigma^{(2)} = m_S^{(2)} \neq 0$, with $m_{\sigma S}^{(2)} > m_{\sigma S}^{(1)}$, this phase is denoted by $\langle \sigma S \rangle^{(2)}$.

(iii) The *Para* phase is denoted by P_3, where $m_\tau^{(1)} = 0$, with $h = 0$. Considering $h > 0$, for $m_\tau^{(2)} \neq 0$, this phase is denoted by *Baxter*$^{(3)}$.

(iv) The region in the diagrams where occur first-order phase transitions between the phases P_1, P_2 and P_3, with values of the external field $h \geq 0$, is denoted by dense phase (d_P).

We will start our discussions by analyzing the phases and magnetizations curves presented by this system, both in the absence and in the presence of an external field. The results obtained will be explored later in the MCE investigation. The inputs and parameters used in this section were chosen with the objective of construct a complete picture of the behavior of the system, so that, besides illustrate some special cases, we have also present the general ones.

In Fig. 1(a), we present the phase diagram of the AT model (T as a function of x), where the phases defined above are shown. Considering ($h = 0$), the results obtained are the solid lines representing continuous phase transitions between the P_1P_2, P_1P_3, and P_2P_3 phases, while the dashed lines represent first-order phase transitions between the P_1P_2 and P_1P_3 phases. The continuous and first-order phase transitions are separated by multicritical points E_1 and E_2, and their values are given, respectively, by $x = 0.251$ and $x = 1.911$. Additionally, we can observe the presence of a bifurcation point, indicated by F, which appears at $x = 1.387$. These phase transitions for ($h = 0$) can be studied in more detail in Ref. [53]. For ($h > 0$), only first-order phase transitions occur for different values of the external field. These phase transitions are present in the shaded region, which has been denoted by dense phases d_P, defined above the dashed line and ending at the dotted line. In Fig. 1(b), is shown the external field (h_C) as a function of the temperature (T_C) and the variable x_C. This set of variables, obtained in the equilibrium condition where $G(m_\tau) = G(m'_\tau)$, establishes the presence of first-order phase transitions in the dense region (d_P), which occur between the points E_1 and E_2. The values of the temperatures (T_C) are present in Table 1. The role of the external field is to decrease the region where first-order phase transitions are present in the system. The value of the external field $h_C = 0.2$ vanishes the phase region of (d_P).

In order to show the first-order phase transitions in the presence of an external field $h \geq 0$, in Fig. 2(a), we plot some magnetization curves ($M \equiv \{m_\tau\}$) as functions of temperature (T), where $m_\sigma = m_S = m_{\sigma S}$, for $x = 1$ and external field values of $h = \{0, 0.05, 0.1, 0.15, 0.197, 0.30, 0.50\}$. These transitions, indicated by vertical lines, were also obtained by means of the equilibrium condition $G(m_\tau) = G(m'_\tau)$ and occur in the ranges of temperatures $7.281 \leq T_{Ci} \leq 7.051$ and external fields of $0 \leq h_{Ci} \leq 0.197$. In Fig. 2(b), we show the free energy of the system as a function of the magnetizations (m_τ), for $x = 1$. As we can observe, the pair of values, denoted by $\lambda_{Ci} = (T_{Ci}, h_{Ci})$, indicate first-order phase transitions that occur with the configurations presented in the previous figure. In this context, the dashed lines represent the free energy for $h = 0$ with different values of temperature ($T \geq T_{C1}$), where a first-order phase transition occur at T_{C1}, being $m_\tau = 0$ the stable state for other values of temperature. In Fig. 2(c), the free energy is represented as a function of the magnetizations with $x = 1$, but, this time, the temperature is chosen to be fixed at T_{C4}. For this configuration, we observe that in the range $0 \leq h < 0.15$ of external field intensities, the magnetizations of the system change in a continuous way (solid line), and, at $h = 0.15$, a first-order phase transition occur (dashed line). In the interval $0.15 < h \leq 0.50$, the magnetizations present continuous changes again. Therefore, when considering the temperature $T = T_{C4}$ for external field $h = 0.15$, we must use the Clausius–Clapeyron equation in the calculations made by means of Eq. (9). Now, we turn our attention to the MCE. At first, we will consider the condition $x = 1$, so that the information obtained in the previous figures can be used. Within this approach, we calculated the variation in the magnetic entropy of the system as a function of temperature when the external field applied to it varies from $h = 0$ to $h = h_{Ci}$. These procedures generate one $-\Delta S_M$ curve for each Δh as a function of temperature, which are plotted in Fig. 2(d). Dashed lines are used in the interval of temperatures where first-order phase transitions are exhibited at certain values of external field, while out of it, we have used solid lines. As expected, due to the presence of first-order phase transitions, when the configuration of the inputs (h and T) reaches the ordered pairs (T_{C1}, h_{C1}), the system exhibits a discontinuity in the magentocaloric potential, resulting in a much higher change in its magnetic entropy with external field variations when compared to the regimes where only continuous phase transitions take place. This behavior extend until the temperature of T_{C5} is reached, where the discontinuity of the order parameter in the phase transition goes to zero and only continuous phase transitions are exhibited. In general, all curves plotted in Fig. 2(d) present similar shapes for small temperatures, i.e., an increasing tendency until the temperature T_{C1} and a decreasing behavior after it, as $T \to \infty$. This type of magnetocaloric potential behavior can be observed in some classes of materials, as can be seen in the work of Skini et al. [78] in which researchers obtained results on the MCE for $La_{0.8-x}\square_x Ca_{0.2}$MnO3, finding discontinuities in magnetization and on the magnetocaloric potencial, or in the work of Guillou and collaborators [79], where a similar behavior was found in the MCE study for Eu_2In. Other experimental works whose MCE properties have

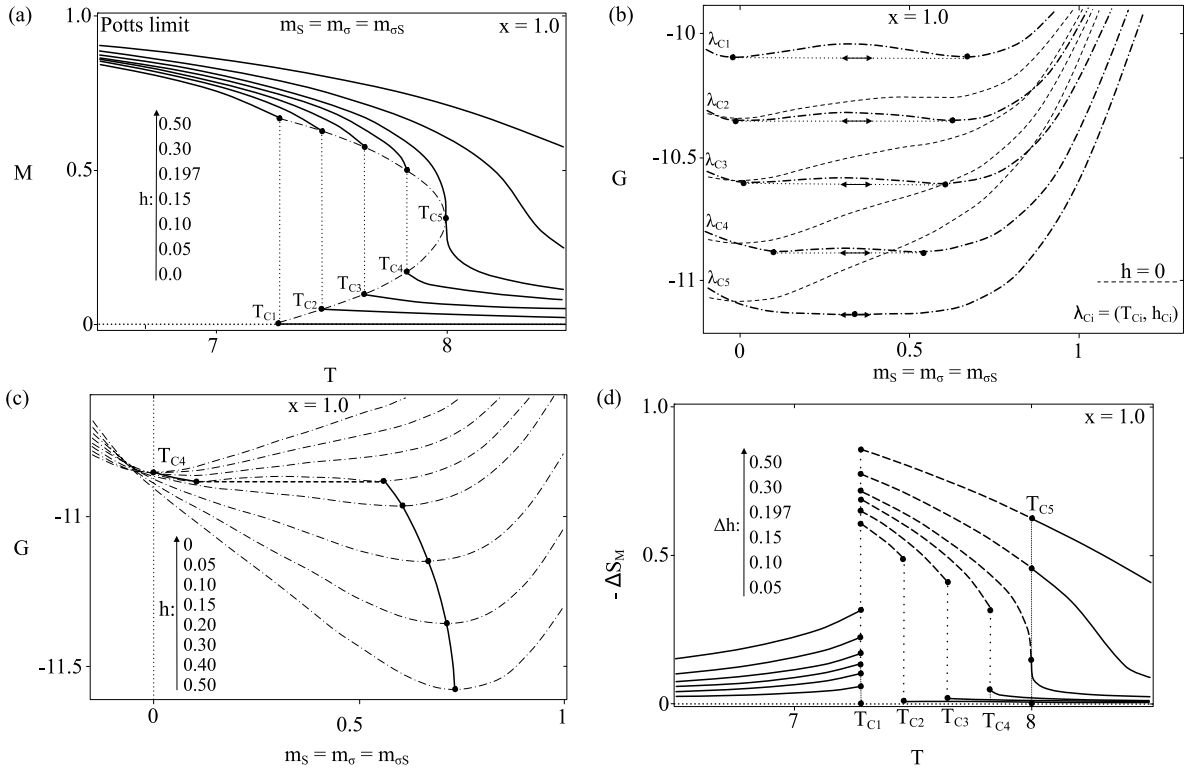

Fig. 2. (a) Magnetization (M) as a function of temperature (T) for $x = 1$ and $h \geq 0$. (b) Free energy (G) as a function of magnetizations ($m_\sigma = m_S = m_{\sigma S}$) for $x = 1$ and $h = 0$, and (c) for $h \geq 0$. (d) Magnetocaloric potential ($-\Delta S_M$) as a function of temperature (T) for $x = 1$ and $\Delta h = \{0.05, 0.10, 0.15, 0.197, 0.30, 0.50\}$.

similarities related to discontinuities in the magnetocaloric potential can be seen in [80–82]. Furthermore, recent theoretical studies have also reported such behavior in the analysis of the MCE, as in the case of the aforementioned works by Oliveira et al. [17], Morais et al. [40] and Nascimento et al. [41], among others [31–33,83].

When $x \neq 1$, the magnetizations m_τ are no longer equal to each other, due to the difference between the couplings J and K, and because of that, the system will present the configurations $m_\sigma = m_S > m_{\sigma S}$ and $m_\sigma = m_S < m_{\sigma S}$ for, let us say, $x = 0.5$ and $x = 1.3$, respectively. It is interesting to analyze how these features impact the magnetocaloric potential curves, so, in the next figures, let us analyze the magnetizations and the $-\Delta S_M$, side by side, for both mentioned values of x.

In Fig. 3(a) and (b), the magnetizations are plotted for external fields given by $h = \{0, 0.036, 0.067, 0.5\}$ and $h = \{0, 0.089, 0.170, 0.5\}$, for $x = 0.5$ and $x = 1.3$, respectively, while in $-\Delta S_M$ curves, the field variation is $\Delta h = 0.5$ in both figures. Here, we can observe similar patterns to that shown in the previous figures, with $-\Delta S_M$ increasing until the temperatures T_{Ci}; in this context, given by T_{C6} and T_{C9}, still increasing the temperatures, the $-\Delta S_M$ starts to decrease, but still showing a high value compared to the regions where no first-order phase transitions are present (solid lines). At T_{C8} and T_{C11}, the system goes out of the first-order phase transition regime, and the magnetocaloric potential goes to zero as $T \to \infty$. In addition, in Fig. 3(c), the magnetizations and the $-\Delta S_M$ are plotted as functions of T, respectively, both for $x = 1.5$. This time, the intensities of the external field related to the magnetization curves are $h = \{0, 0.037, 0.095, 0.5\}$, while its variation in the magnetocaloric potential study is $\Delta h = 0.5$. In this context, the system pass through the phases P_1, P_2 and P_3 (please, see Fig. 1(a)). To verify it, we can observe the magnetization curves when $h = 0$, in which $m_\sigma = m_S < m_{\sigma S} \neq 0$ at T_{C12}, where a first-order phase transition occurs and the magnetizations change from $m_\sigma = m_S$ to zero and from $m_{\sigma S}$ to $m'_{\sigma S} > 0$, i.e., from P_1 to P_2. Then, increasing the temperature until T_{C15} makes the system undergoes a continuous phase transition, going from P_2 to P_3. For the $-\Delta S_M$ curve, the same behavior of previous figures can be observed, with the addition of a peak at T_{C15} due to the continuous phase transition in the order parameter. With the aim of provide a general picture of the magnetocaloric potential behavior, in Fig. 3(d), we plot the $-\Delta S_M$ as a function of T, with external field variation $\Delta h = 0.5$, for $x = \{0, 0.251, 0.5, 0.8, 1.0, 1.3, 1.5, 1.911\}$. Among these values of x, we have some special ones, being $x = 0$ and $x = 1.0$, corresponding to the Ising and Potts limits, respectively, while 0.251 and 1.911 correspond to the points E_1 and E_2 present in the phase diagram where the first-order transition ceases to manifest for a system under null external field. As we can observe, due to continuous phase transitions, some peaks are present in the curves. This behavior was also observed in experimental works, as in the work of Shahumi et al. [84] in which in addition to structural and magnetic properties, the MCE of $La_{0.7}Sr_{0.3}Mn_{1-x}Fe_xO_3$ nanoparticles was studied, obtaining a similar behavior of the magnetocaloric potential to that described above. We can also mention the work of Taubel et al. [85], in which it is also possible to observe these peaks in the magnetocaloric potential related to continuous transitions for all-d-metal Ni – Co – Mn – Ti Heusler alloys under certain conditions. Furthermore, other research that also presented results containing this type of MCE behavior can be seen at [17,31–33,40,41,82,83,86]. Still in relation to the analysis of Fig. 3(d), the presence of a double peak for some values of x and T is observed. This pattern of magnetocaloric potential behavior has also been observed by Ivchenko and Igoshev [87] in their work on MCE in metallic systems with the presence of first-order transitions and in the work of Nascimento et al. [41] in their work on MCE in the Blume–Capel spin-3/2 model. According to these studies, this pattern seems to be related to systems whose temperatures T_C are variable. Another study that also observed the presence of this pattern of double peaks in the MCE was that of Yüksel [88], in which through the analysis of morphological, magnetic and magnetocaloric properties of ferromagnetic nanoparticles with core–shell geometry the author defined that the presence of these double peaks in the magnetocaloric

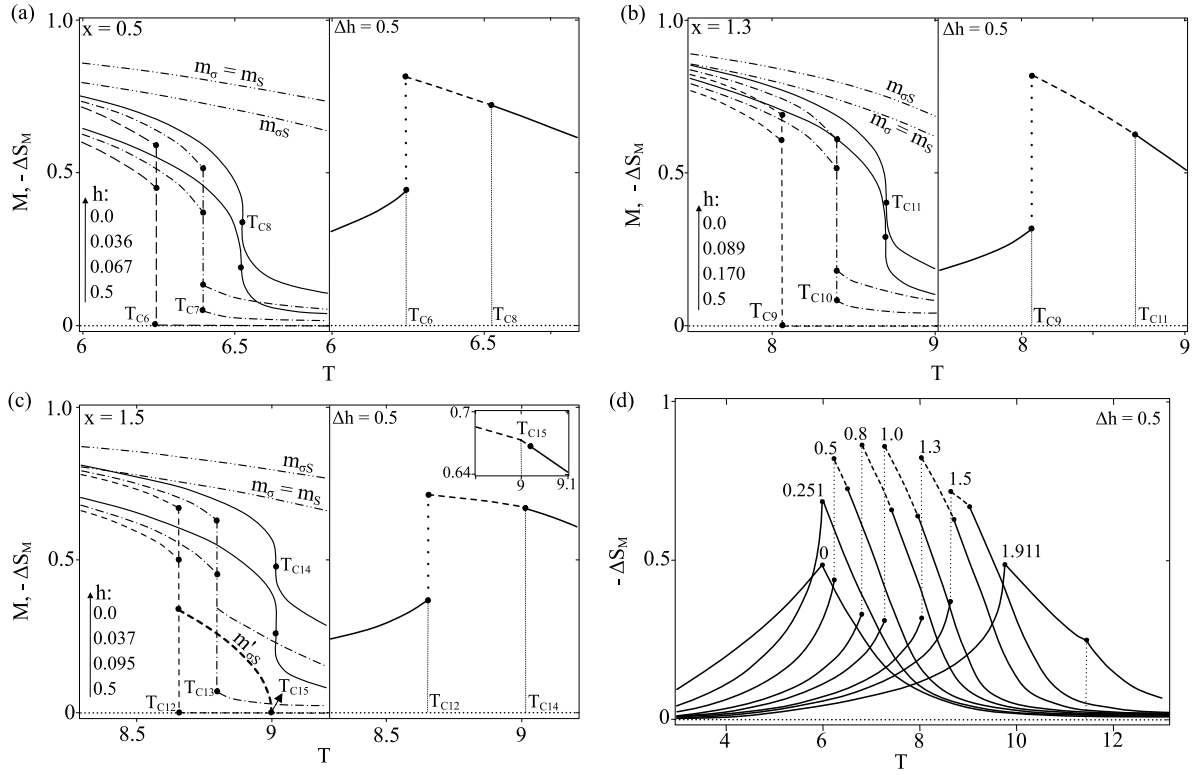

Fig. 3. In figures (a), (b), and (c), the magnetization and MCE diagrams are shown as a function of temperature for values of $x = \{0.5, 1.3, 1.5\}$. In figure (d), the MCE diagram is presented as a function of temperature for values of x ranging from $x = 0$ to the limit where the first-order phase transition ends at $x = 1.911$.

potential defined through the magnetic entropy change of the system are associated with two phase transitions, one related to the core layer and the other related to the shell layer.

In this context, when x is equal to 0 until 0.251, the peaks occur at the phase transition between the P_1 and P_3 phases, while when $x = 1.911$, there are peaks where the system changes from the P_1 to the P_2 and from the P_2 to the P_3 phases. For x values that lies between E_1 and E_2, the system present first-order phase transitions, so that we can observe discontinuities in the $-\Delta S_M$ curves. This region, depicted by a dashed line, represent the most favorable regime for magnetocaloric potential measurements because of its high values compared to regions where only continuous phase transitions are presented.

To finalize our study, let us analyze the results of the MCE for the spin-1/2 AT model, for $x = 1$, considering phase transitions that occur between metastable and stable states due to the hysteresis effect when varying the external field. In Fig. 4(a), we have some magnetization curves with the same configuration of Fig. 2(a). The difference here is the presence of metastable (dashed lines) and unstable (dotted lines) states in the diagram, in which the vertical dotted lines indicate the temperatures where first-order phase transitions occur between stable states, where the presence of double arrows means that the phase transition can occur in both ways, i.e., from higher to lower magnetization values and vice versa. Regarding the hysteresis effect, the vertical arrows (↑) that initiate at $T = 6.0$ and end at T_{C5} represent phase transitions from metastable (lower magnetization) to stable (higher magnetization) states, while the vertical arrows (↓) that initiate at T_{C16} and last until T_{C5} represent the same type of phase transition, but in the opposite way. In Fig. 4(b), by means of the free energy (G) of the system, we can verify these phase transitions with more details. In this diagram, in order to give an example for illustration purposes, we have set $T = T_{C16}$ and $x = 1$, such that, for values of external field starting at $h = 0$ until $h = 0.095$, the local minimum of G (metastable state) disappears, making the system reach the stable state by means of hysteresis effects in both cases. When $h = 0.048$, the system undergoes a first-order phase transition between stable states (equilibrium condition $G(m_\tau) = G(m'_\tau)$), as were indicated in the magnetization curves. The free energy of the system for $x = 1$ and $h = 0$ can be analyzed with more details in Ref. [53]. In Fig. 4(c) e (d), where $-\Delta S_M$ is shown as a function of T, with external field variations of $0 \leq h \leq 0.5$ and $0 \leq h \leq 2.0$, respectively, we will explore the phase transitions described in Fig. 4(a) and (b). In these diagrams, the line between T_{C1} and T_{C5} was obtained via Eqs. (5) and (7), where phase transitions between stable states are present (↕). For phase transitions driven by hysteresis from highly magnetized metastable to slightly magnetized stable states, we have the dashed-dotted line between T_{C16} and T_{C5}, obtained by means of the Maxwell relations (Eq. (9)), besides the dashed line between the points Q_1 and T_{C5}, obtained via entropy variation (Eq. (7)). For the same kind of phase transition, but going from slightly magnetized metastable to highly magnetized stable states, we have also the dashed-dotted line between Q_2 and T_{C5} and the dashed line between Q_3 and T_{C5}, calculated by means of the Maxwell relations and the entropy variation, respectively. As we can observe in Fig. 4(c), where $0 \leq h \leq 0.5$, the results obtained via Eqs. (7) and (9) for the phase transitions between metastable and stable states are not equal to each other. Besides that, in Fig. 4(d), for $0 \leq h \leq 2.0$, we note that at T_{C16} the magnetocaloric potential of the system reaches values that are higher than the maximum entropy of the spin-1/2 AT model (ln(4)), while at Q_3, this error do not occur. These facts evidence what had already been observed by Amaral et al. [76], i.e., that the Maxwell relations cannot be used to investigate MCE effects in non-equilibrium systems.

4. Conclusions

In this work we have investigated the magnetic and magnetocaloric properties of the spin-1/2 Ashkin-Teller model in a cubic lattice under an external field potential under conditions of different lattice parameters and system stability levels. The numerical results were obtained by means of the Mean Field Theory approximation through

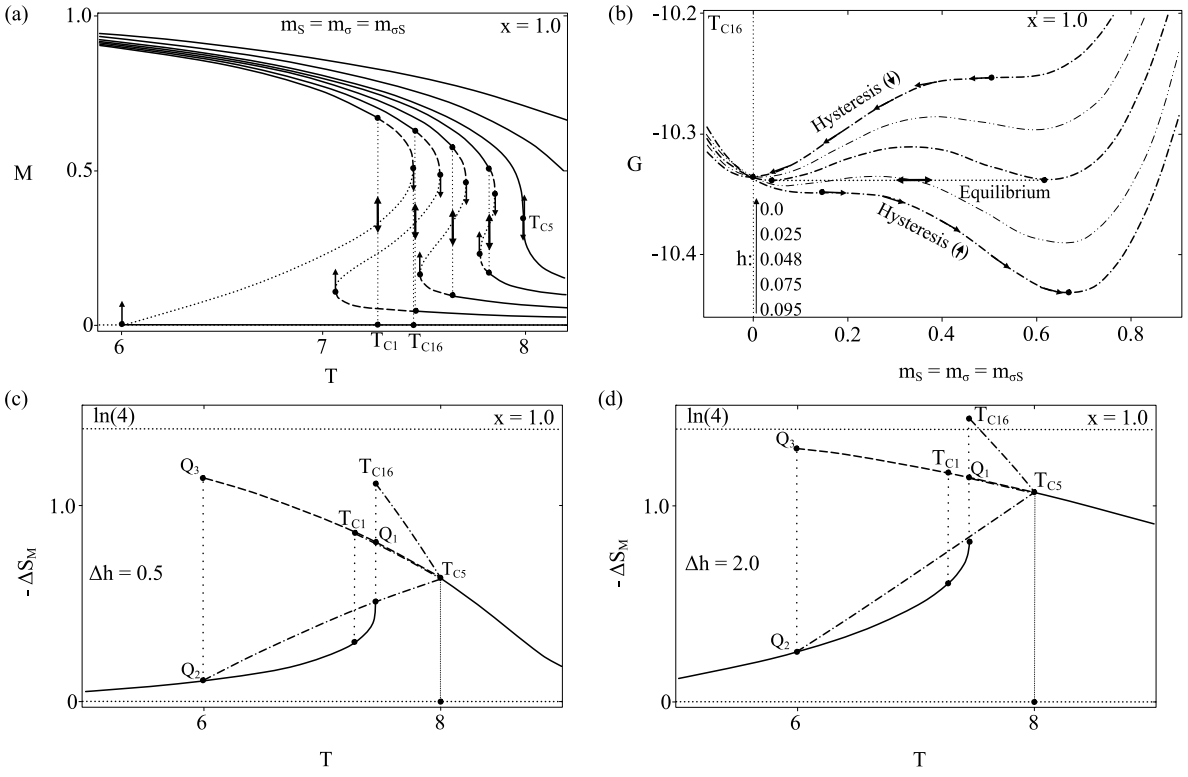

Fig. 4. (a) Magnetization (M) as function of temperature (T) for $x = 1$ and $h = 0$. (b) Free energy (G)as a function of magnetizations with T_{C16} held constant and $h \geq 0$. (c) $-\Delta S_M$ as a function of (T) for $x = 1$ and $\Delta h = 0.5$, (d) for $\Delta h = 2.0$, highlighting the inadequacy of the Maxwell relations in the study of magnetocaloric potential, where the model exhibits first-order phase transitions, as observed previously by Amaral et al. [76].

Table 1
For numerical comparison and experimental propose, we show some values of temperatures T_{Ci} discussed in this section.

Notation	Value	Notation	Value	Notation	Value	Notation	Value
T_{C1}	7.281	T_{C5}	7.999	T_{C9}	8.068	T_{C13}	8.800
T_{C2}	7.463	T_{C6}	6.246	T_{C10}	8.400	T_{C14}	9.015
T_{C3}	7.646	T_{C7}	6.400	T_{C11}	8.700	T_{C15}	8.999
T_{C4}	7.828	T_{C8}	6.526	T_{C12}	8.656	T_{C16}	7.456

the Bogoliubov inequality, showing convergence with experimental and theoretical works such as [17,31–33,40,41,82,83,86], in addition to new informations about the system under analysis.

The Ashkin-Teller model presents two distinct coupling constants that could be explained as two Ising models in contact with each other. Those two Ising models presents self (J) and inter-couplings (K) and this open the possibilities of having regions where the self coupling parameter is bigger, smaller and equal in magnitude compared to the inter-coupling one. The results presented in this work showed that the weight between the two coupling parameters could potentially leads to situations where changing the temperature, at first under zero external fields, produce continuous or first-order phase transitions. In the case of equal magnitude, that is $J/K = 1$, the results showed that the Asking-Teller model presents first-order phase transitions at zero external magnetic field. Another result presented was that first-order phase transitions favor high variations in the magnetocaloric potential. When analyzing the results, we also realized that the action of the external field increases the value of the temperature T_C where the first order transition takes place, whereas its action also presents a critical point where the first order transition vanishes from the system and only continuous transitions remain.

The system configuration where the magnitude of the self-coupling (J) are bigger or smaller than the inter-coupling (K) also present first-order phase transitions, once again this behavior favors the MCE. The point where $K/J = 0.251$ or $K/J = 1.911$ are specially important due to the fact that for zero external field the first-order transition are no longer placed in the system, only continuous transitions are numerically observable. In this case, the results suggest that the magnetocaloric potential would be less efficient for materials with similar properties. In both couplings configurations, that is, the ratio K/J being bigger or smaller than one, the effect of applying a magnetic field in the system tends to increase the temperature where the first-order transitions are present, except for the couplings configurations where the first-order transitions vanishes.

The AT model still corroborates with a system configuration where continuous and first-order phase transitions manifest simultaneously. For system configurations where $1.387 \ll K/J \ll 1.5$ a bifurcation point is characterized. The experimental possibilities around this behavior regardless to the MCE are very exciting, although the finding of the present work suggest that the system of configuration around $K/J = 1$ are more prominent to produce system with better MCE properties.

Finally, for a system configuration of $K/J = 1$, we highlighted the phase transitions between metastable and stable states due to the hysteresis effect under the action of an external magnetic field. Beyond mapping the stable and metastable states transition, where the first-order transition happens, we proved the findings of Amaral and collaborators [76] through a convergence of results. There he showed the fail of Maxwell relations in order to investigate the MCE effects in non-equilibrium states. Instead, here we suggest the use of entropy variation to compute the correct MCE properties.

CRediT authorship contribution statement

J.P. Santos: Writing – review & editing, Writing – original draft, Supervision, Methodology, Formal analysis, Conceptualization. **R.H.M. Morais:** Writing – review & editing, Software, Methodology, Formal analysis. **R.M. Francisco:** Writing – original draft, Software, Methodology. **D.S. Rosa:** Validation, Software, Methodology, Investigation.

E. Nepomuceno: Writing – review & editing, Validation, Supervision, Formal analysis, Conceptualization.

Declaration of competing interest

The authors declare that they have no known competing financial interests or personal relationships that could have appeared to influence the work reported in this paper.

Data availability

No data was used for the research described in the article.

Acknowledgments

J. P. Santos would like to thank the Conselho Nacional de Desenvolvimento Científico e Tecnológico - CNPq, Brazil (No. 304101/2022-2) for financial support. R. H. M. Morais acknowledges that this study was financed in part by the Coordenação de Aperfeiçoamento de Pessoal de Nível Superior - Brasil (CAPES) - Finance Code No. 88887.710839/2022-00. R. M. Francisco acknowledges the support of the São Paulo Research Foundation (FAPESP), Brazil Grant No. 2023/08600-9. D. S. Rosa acknowledges the support of the São Paulo Research Foundation (FAPESP), Brazil Grant No. 2023/02261-8.

Funding

This research received no external funding.

References

[1] E. Warburg, Magnetische untersuchungen, Ann. Phys. 249 (141) (1881).
[2] P. Weiss, A. Piccard, Sur un nouveau phènoméne magnétocalorique, Les C. R. l Acad. Des Sci. 166 (1918) 325.
[3] V.K. Pecharsky, K.A. Gschneidner Jr., Magnetocaloric effect from indirect measurements: Magnetization and heat capacity, J. Appl. Phys. 86 (1999) 565.
[4] A.I. Guerrero, Magnetocaloric effect in the $J_x J_y$ Blume–Capel model, Phys. A 623 (2023) 128892.
[5] S. Mandal, S. Mohanty, S. Mukherjee, Theoretical investigation of direct and inverse magnetocaloric effect in $La_2FeMn_{1-x}Cu_xO_6$ and $Sr_2RuMn_{1-x}Fe_xO_6$ using a phenomenological model, Solid State Commun. 366 (2023) 115159.
[6] B. Alzahrani, M. Hsini, S. Hcini, M. Boudard, A. Dhahri, M.L. Bouazizi, Study of the magnetocaloric effect by means of theoretical models in $La_{0.6}Ca_{0.2}Na_{0.2}MnO_3$ manganite compound, J. Low Temp. Phys. 200 (2020) 26.
[7] K. Szałowski, P. Kowalewska, Magnetocaloric effect in Cu_5-NIPA molecular magnet: A theoretical study, Materials 13 (2020) 485.
[8] S. El Ouahbi, Magneto-caloric effect simulated by landau theory in amorphous $Fe_{28}Y_{52}B_{20}$ alloy, J. Supercond. Nov. Magn. 35 (2022) 2859.
[9] C. Ekiz, Thermodynamic properties and magnetocaloric effect in dendrimer-like recursive lattice, Phys. A 626 (2023) 129088.
[10] S. Ghorai, R. Skini, D. Hedlund, P. Ström, P. Svedlindh, Field induced crossover in critical behaviour and direct measurement of the magnetocaloric properties of $La_{0.4}Pr_{0.3}Ca_{0.1}Sr_{0.2}MnO_3$, Sci. Rep. 10 (2020) 19485.
[11] P. Sharmaa, R. Masrour, A. Jabar, J. Fana, A. Kumar, L. Ling, C. Ma, C. Wang, H. Yang, Structural and magnetocaloric properties of rare-earth orthoferrite perovskite: $TmFeO_3$, Chem. Phys. Lett. 740 (2020) 137057.
[12] M. Bouhbou, R. Moubah, A. Džubinská, M. Reiffers, V. Tuyikeze, A. Natik, F. Fraija, H. Lassri, Magnetic,magnetocaloric and critical exponent properties of amorphous $Fe_{67}Y_{33}$ ribbons prepared by melt-spinning technique, Phys. A 534 (2019) 122088.
[13] Y.C. Zhanga, F.X. Qina, D. Esteveza, V. Francob, H.X. Peng, Structure, magnetic and magnetocaloric properties of Ni_2MnGa Heusler alloy nanowires, J. Magn. Magn. Mater. 513 (2020) 167100.
[14] M. Saidi, S. Walha, E.K. Hlil, L. Bessais, M. Jemmali, Effect of chromium substitution on structural, magnetic and magnetocaloric properties of $GdFe_{12-x}Cr_x$ intermetallic compounds, Mössbauer spectrometry and ab initio calculations, J. Solid State Chem. 297 (2021) 122019.
[15] M. Jeddi, H. Gharsallah, M. Bekri, E. Dhahri, E.K. Hlil, Structural, Magnetic and magnetocaloric properties of $0.75La_{0.6}Ca_{0.4}MnO_3/0.25La_{0.6}Sr_{0.4}MnO_3$ nanocomposite manganite, RSC Adv. 8 (2018) 28649.
[16] A. Elouafi, R. Moubah, S. Derkaoui, A. Tizliouine, R. Cherkaoui, S. Shi, A. Bendani, M. Sajieddine, H. Lassri, Finite size effects on the magnetocaloric properties around blocking temperature in $\gamma - Fe_2O_3$ nanoparticles, Phys. A 523 (2019) 260.
[17] S. Oliveira, R.H.M. Morais, J.P. Santos, F.C. Sá Barreto, Theoretical analysis of magnetic properties and the magnetocaloric effect using the Blume–Capel model, Condens. Matter Phys. 25 (2022) 13702.
[18] M.S.M. Abu-Elmagd, T. Hammad, A. Abdel-Kader, N. El-Shamy, S. Yehia, S.H. Aly, F.Z. Mohammad, First principles and mean field study on the magnetocaloric effect of YFe_3 and $HoFe_3$ compounds, Sci. Rep. 13 (2023) 2876.
[19] A. Mounira, N.Zaidi, E.K. Hlil, Magnetocaloric effect simulation in $TbFeSi$ and $DyFeSi$ intermetallic magnetic alloys using mean-field model, J. Supercond. Nov. Magn. 36 (2023) 397.
[20] Y. Yüksel, E. Vatansever, Ü. Akinci, Magnetocaloric properties of the spin-s ($S \geqslant 1$) ising model driven by a time dependent oscillating magnetic field, Phys. Lett. A 388 (2021) 127079.
[21] S. Khadhraoui, N. Khedmi, M. Hsini, Studying the magnetocaloric effect in $Nd_{0.55}Sr_{0.45}MnO_3$ manganite by the mean-field model, J. Supercond. Nov. Magn. 34 (2021) 1495.
[22] M. Hsini, S. Hcini, S. Zemni, Magnetocaloric effect studying by means of theoretical models in $Pr_{0.5}Sr_{0.5}MnO_3$ manganite, J. Magn. Magn. Mater. 466 (2018) 368.
[23] M. Hsini, S. Hcini, S. Zemni, Magnetocaloric effect simulation by landau theory and mean-field approximation in $Pr_{0.5}Sr_{0.5}MnO_3$, Eur. Phys. J. Plus 134 (2019) 588.
[24] A. Belkahla, K. Cherif, H. Belmabrouk, A. Bajahzar, J. Dhahri, E.K. Hlil, Study of mean-field theory on the magnetocaloric effect of $La_{0.7}Bi_{0.05}Sr_{0.15}Ca_{0.1}Mn_{0.85}In_{0.15}O_3$ manganite, Appl. Phys. A 125 (2019) 1.
[25] C. Henchiri, A. Benali, T. Mnasri, M.A. Valente, E. Dhahri, Modeling the magnetocaloric effect of $La_{0.8}MnO_3$ by the mean-field theory, J. Supercond. Nov. Magn. 33 (2020) 1143.
[26] M. Khlifi, J. Dhahri, E. Dhahri, E.K. Hlil, Modeling of magnetic and magnetocaloric properties by the molecular mean field theory in $La_{0.8}Ca_{0.2}MnO_3$ oxides with first and second magnetic phase transition, J. Magn. Magn. Mater. 480 (2019) 1.
[27] R.H.M. Morais, J.P. Santos, F.C. Sá Barreto, The q-state potts model on a nanostructure of hexagonal lattices with ABA stacking, Phys. B 627 (2022) 413512.
[28] Ü. Akıncı, Magnetocaloric properties of the binary ising model with arbitrary spin, J. Magn. Magn. Mater. 523 (2021) 167625.
[29] Y.G. Yildiz, G.D. Yildiz, Modeling of the magnetization and magnetocaloric effect in Ni_2MnGa Heusler alloy with the effective field theory, J. Low Temp. Phys. 207 (2022) 171.
[30] Y. Yüksel, Ü. Akinci, A comparative study of critical phenomena and magnetocaloric properties of ferromagnetic ternary alloys, J. Phys. Chem. Solids 112 (2018) 143.
[31] E. Vatansever, Ü. Akinci, Y. Yüksel, Non equilibrium magnetocaloric properties of ising model defined on regular lattices with arbitrary coordination number, Phys. A 479 (2017) 563.
[32] Y. Yüksel, Ü. Akıncı, E. Vatansever, Influence of modified surface effects on the magnetocaloric properties of ferromagnetic thin films, Thin Solid Films 646 (2018) 67.
[33] Ü. Akinci, Y. Yüksel, E. Vatansever, Magnetocaloric properties of the spin-s ($S \geqslant 1$) ising model on a honeycomb lattice, Phys. Lett. A 382 (2018) 3238.
[34] G. Kadim, R. Masrour, A. Jabar, E.K. Hlil, Room-temperature large magnetocaloric, electronic and magnetic properties in $La_{0.75}Sr_{0.25}MnO_3$ manganite: Ab initio calculations and Monte Carlo simulations, Phys. A 573 (2021) 125936.
[35] M. Yang, F. Wang, J.Q. Lv, B.C. Li, W. Wang, Thermodynamic properties and magnetocaloric effect of a polyhedral chain: A Monte Carlo study, Phys. B 638 (2020) 413954.
[36] G. Kadim, R. Masrour, A. Jabar, Large.magnetocaloric. effect, Magnetic and electronic properties in Ho_3Pd_2 compound: Ab initio calculations and Monte Carlo simulations, J. Magn. Magn. Mater. 499 (2020) 166263.
[37] G. Kadim, R. Masrour, A. Jabar, Magnetocaloric effect, electronic and magnetic properties of Ba1-xSrxFeO3 barium-strontium ferrites: Monte Carlo simulations and comparative study between TB-mBJ and GGA+U, Mater. Today Commun. 26 (2021) 102071.
[38] R. Masrour, A. Jabar, H. Khlif, F.B. Jemaa, M. Ellouze, E.K. Hlil, Experiment, mean field theory and Monte Carlo simulations of the magnetocaloric effect in $La_{0.67}Ba_{0.22}Sr_{0.11}MnO_3$ compound, Solid State Commun. 268 (2017) 64.
[39] F. Zhang, K. Westra, Q. Shen, I. Batashev, A. Kiecana, N. van Dijk, E. Brück, The second-order magnetic phase transition and magnetocaloric effect in all-d-metal $NiCoMnTi$-based Heusler alloys, J. Alloys Compd. 906 (2022) 164337.
[40] R.H.M. Morais, J.P. Santos, S. Oliveira, R.G.B. Mendes, D.S. Rosa, R.M. Francisco, F.C. Sá Barreto, Magnetocaloric effect in the potts model based on the effective-field theory, Phys. Lett. A 424 (2022) 127844.
[41] G.B.B. Nascimento, V.T.P. Vieira, R.H.M. Morais, S. Oliveira, J.P. Santos, Study of the magnetocaloric effect and magnetic properties in the spin-3/2 Blume–Capel model, J. Magn. Magn. Mater. 588 (2023) 171467.
[42] E.E. Kokorina, M.V. Medvedev, Magnetocaloric effect in a first-order phase transition in a ferromagnet with biquadratic exchange, Phys. Met. Metallogr. 122 (2021) 1045.

[43] A. Biswas, R.K. Chouhan, A. Thayer, Y. Mudryk, I.Z. Hlova, O. Dolotko, V.K. Pecharsky, Unusual first-order magnetic phase transition and large magnetocaloric effect in Nd_2In, Phys. Rev. Mater. 6 (2022) 114406.

[44] A.D. García, J.Y. Law, L.M.M. Ramírez, A.K. Giri, V. Franco, Deconvolution of overlapping first and second order phase transitions in a $NiMnIn$ Heusler alloy using the scaling laws of the magnetocaloric effect, J. Alloys Compd. 871 (2021) 159621.

[45] V.I. Val'kov, V.I. Kamenev, A.V. Golovchan, I.F. Gribanov, V.V. Koledov, V.G. Shavrov, V.I. Mitsiuk, P. Duda, Magnetic and magnetocaloric effects in systems with reverse first-order transitions, Phys. Solid State 63 (2021) 1889.

[46] S. Ghosh, S. Ghosh, Giant magnetocaloric effect driven by first-order magnetostructural transition in cosubstituted $Ni-Mn-Sb$ Heusler compounds: Predictions from ab initio and Monte Carlo calculations, Phys. Rev. B 103 (2021) 054101.

[47] J. Ashkin, E. Teller, Statistics of two-dimensional lattices with four components, Phys. Rev. 64 (1943) 178.

[48] Z. Wojtkowiak, G. Musiał, The behavior of the three-dimensional Askin–Teller model at the Mixed Phase Region by a new Monte Carlo approach, J. Stat. Phys. 189 (2022) 3.

[49] I. Keçoğlu, A.N. Berker, Global Ashkin–Teller phase diagrams in two and three dimensions: Multicritical bifurcation versus double tricriticality—endpoint, Phys. A 630 (2023) 129248.

[50] M. Sluiter, Y. Kawazoe, Magnetism and chemical interactions in metallic alloys, Sci. Rep. RITU A 40 (1995) 301.

[51] C. Zhe, W. Ping, Z.Y. Hong, Ashkin–Teller formalism for elastic response of DNA molecule to external force and torque, Commun. Theor. Phys. (Beijing) 49 (2008) 525.

[52] P. Bak, P. Kleban, W.N. Unertl, J. Ochab, G. Akinci, N.C. Bartelt, T.L. Einstein, Phase diagram of selenium adsorbed on the Ni (100) surface: A physical realization of the Ashkin-Teller model, Phys. Rev. Lett. 54 (1985) 14.

[53] J.P. Santos, J.A.J. Avila, D.S. Rosa, R.M. Francisco, Multicritical phase diagram of the three-dimensional Ashkin-Teller model including metastable and unstable phases, J. Magn. Magn. Mater. 469 (2019) 35.

[54] R.V. Ditzian, R.J. Banavar, G.S. Grest, L.P. Kadanoff, Phase diagram for the Ashkin-Teller model in three dimensions, Phys. Rev. B 22 (1980) 2542.

[55] P.L. Christiano, S.G. Rosa, Mean-field theory of the Ashkin-Teller spin glass, Phys. Rev. A 34 (1986) 730.

[56] J.P. Santos, D.S. Rosa, F.C. Sá Barreto, New Baxter phase in the Ashkin–Teller model on a cubic lattice, Phys. Lett. A 382 (2018) 272.

[57] J.P. Santos, G.B.B. Nascimento, K.L.A. Resende, R.M. Francisco, Phase diagrams and magnetization curves of the mixed Ashkin–Teller model including metastable and unstable states, Eur. Phys. J. B 94 (2021) 136.

[58] R.M. Francisco, J.P. Santos, Magnetic properties of the Ashkin–Teller model on a hexagonal nanotube, Phys. Lett. A 383 (2018) 1092.

[59] J.P. Santos, F.C. Sá Barreto, New effective field theory for the Ashkin–Teller model, Phys. A 421 (2015) 316.

[60] J.P. Santos, F.C. Sá Barreto, Upper bounds on the critical temperature of the Ashkin-Teller model, Braz. J. Phys. 46 (2016) 70.

[61] N. Benayad, A. Benyoussef, N. Boccara, A.E. Kenz, Renormalisation group recursion relations using the application of generalised callen identities to the Ashkin-Teller model, J. Phys. C 21 (1988) 5747.

[62] P.M.C. Oliveira, F.C. Sá Barreto, Renormalization group studies of the Ashkin-Teller model, J. Stat. Phys. 57 (1989) 53.

[63] J.A. Plascak, F.C. Sá Barreto, Critical properties of the Ashkin-Teller model from the mean-field renormalisation group approach, Phys. A 19 (1986) 2195.

[64] P. Pawlicki, G. Musial, G. Kamieniarz, J. Rogiers, Mean field renormalization group study of a modified Ashkin-Teller model, Phys. A 242 (1997) 281.

[65] G. Musiał, D.J. Knioła, Z. Wojtkowiak, Monte Carlo examination of first-order phase transitions in a system with many independent order parameters: Three-dimensional Ashkin-Teller model, Phys. Rev. E 103 (2021) 062124.

[66] Z. Wojtkowiak, G. Musial, Cluster Monte Carlo method for the 3D Ashkin–Teller model, J. Magn. Magn. Mater. 500 (2020) 166365.

[67] D.J. Kniola, Z. Wojtkowiak, G. Musial, Computation of latent heat based on the energy distribution histogram in the 3D Ashkin-Teller model, Acta Phys. Pol. A 133 (2018) 435.

[68] Ü. Akıncı, Nonequilibrium phase transitions in isotropic Ashkin–Teller model, Phys. A 469 (2017) 740.

[69] J.P. Santos, R.M. Francisco, D.S. Rosa, Dynamic magnetic properties and multicritical phase diagram of the spin-1/2 Ashkin-Teller model under a time dependent external field, J. Magn. Magn. Mater. 538 (2021) 168281.

[70] A. Benmansour, S. Bekhechi, B.E.N. Brahmi, N. Moussa, H.E. Zahraouy, Magnetic properties and phase diagrams of the spin-1 Ashkin Teller model ferromagnetic thin films in the presence of a crystal field, Chinese J. Phys. 74 (2021) 82.

[71] A. Kumar, J.G.M. Guy, L. Zhang, J. Chen, J.M. Gregg, J.F. Scott, Nanodomain patterns in ultra-tetragonal lead titanate ($PbTiO_3$), Appl. Phys. Lett. 116 (2020) 182903.

[72] C.M. Varma, L. Zhu, Specific heat and sound velocity at the relevant competing phase of high-temperature superconductors, Proc. Natl. Acad. Sci. USA 112 (2015) 6331.

[73] N. Bogoliubov, On the theory of superfluidity, J. Phys. 11 (1947) 23.

[74] R.P. Feynman, Slow electrons in a polar crystal, Phys. Rev. 97 (1955) 660.

[75] H. Falk, Inequalities of JW gibbs, Am. J. Phys. 38 (1970) 858.

[76] J.S. Amaral, V.S. Amaral, On estimating the magnetocaloric effect from magnetization measurements, J. Magn. Magn. Mater. 322 (2010) 1552.

[77] A.M. Tishin, Y.I. Spichkin, The Magnetocaloric Effect and Its Applications, CRC Press, 2016.

[78] R. Skini, A. Omri, M. Khlifi, E. Dhahri, E.K. Hlil, Large magnetocaloric effect in lanthanum-deficiency manganites $La_{0.8-x}\square_x Ca_{0.2}MnO3$ ($0.00 \geq x \leq 0.20$) with a first-order magnetic phase transition, J. Magn. Magn. Mater. 364 (2014) 5.

[79] F. Guillou, A.K. Pathak, D. Paudyal, Y. Mudryk, F. Wilhelm, A. Rogalev, V.K. Pecharsky, Non-hysteretic first-order phase transition with large latent heat and giant low-field magnetocaloric effect, Nat. Commun. 9 (2018) 2925.

[80] Z. Song, Z. Li, B. Yang, H. Yan, C. Esling, X. Zhao, L. Zuo, Large low-field reversible magnetocaloric effect in itinerant-electron $Hf_{1-x}Ta_xFe_2$ alloys, Materials 14 (2021) 5233.

[81] E. Palacios, R. Burriel, C.L. Zhang, Calorimetric study of the giant magnetocaloric effect in $(MnNiSi)_{0.56}(FeNiGe)_{0.44}$, Phys. Rev. B 103 (2021) 104402.

[82] H. Wada, K. Taniguchi, Y. Tanabe, Extremely large magnetic entropy change of $MnAs_{1-x}Sb_x$ near room temperature, Mater. Trans. 43 (2002) 73.

[83] N.A. de Oliveira, P.J. von Ranke, Theoretical aspects of the magnetocaloric effect, Phys. Rep. 489 (2010) 89.

[84] T.M. Al-Shahumi, I.A. Al-Omari, S.H. Al-Harthi, M.T.Z. Myint, P. Kharel, S. Lamichhane, S.H. Liou, Synthesis, structure, morphology, magnetism, and magnetocaloric-effect studies of $La_{0.7}Sr_{0.3}Mn_{1-x}Fe_xO_3$ perovskite nanoparticles, J. Alloys Compd. 958 (2023) 170454.

[85] A. Taubel, B. Beckmann, L. Pfeuffer, N. Fortunato, F. Scheibel, S. Ener, T. Gottschall, K.P. Skokov, H. Zhang, O. Gutfleisch, Tailoring magnetocaloric effect in all-d-metal $Ni-Co-Mn-Ti$ Heusler alloys: a combined experimental and theoretical study, Acta Mater. 201 (2020) 425.

[86] G.J. Liu, J.R. Sun, J. Shen, B. Gao, H.W. Zhang, F.X. Hu, B.G. Shen, Determination of the entropy changes in the compounds with a first-order magnetic transition, Appl. Phys. Lett. 90 (2007) 032507.

[87] V.V. Ivchenko, P.A. Igoshev, Emerging mechanisms of magnetocaloric effect in phase-separated metals, Phys. Rev. B 104 (2021) 024425.

[88] Y. Yüksel, The effect of interfacial morphology on the magnetic and magnetocaloric properties of ferromagnetic nanoparticles with core–shell geometry: a Monte Carlo study, Turk. J. Phys. 46 (2022) 27.